31st Congress of the International Council of the Aeronautical Sciences

Belo Horizonte, Brazil; September 09-14, 2018

NUMERICAL HIGH LIFT PREDICTION ON THE JAXA STANDARD MODEL

Vincenzo Cusati*, Pierluigi Della Vecchia*, Danilo Ciliberti*, Salvatore Corcione*, Fabrizio Nicolosi*

***University of Naples "Federico II", DAF Research Group, Dept. of Industrial Eng., 21 Via Claudio, 80125, Naples, Italy**

Keywords: *aerodynamics, high lift, CFD*

Abstract

A growing interest in the prediction of high lift aerodynamics has grown in recent years, motivated by the AIAA High Lift Prediction Workshop (HiLiftPW) series, which publicly release standard wing-fuselage geometries with experimental results from wind tunnel tests and promote dissemination of meshing strategies, physics modelling, and statistical analyses on the results provided by participants. The object of this work is the JAXA standard model proposed in the 3rd AIAA HiLiftPW. The authors want to propose best practices for numerical meshing and analysis with the lowest possible number of cells, giving indications on physics modelling and on the location of grid refinements for mesh tuning.

1 Introduction

Nowadays the numerical, high lift, aerodynamic analysis of commercial aircraft configurations is a crucial item to reduce the number of wind tunnel tests and give a well-suited instrument for the industrial design of the high lift systems. These numerical simulations are very complex, due to difficulties to simulate separations phenomena, unsteadiness, confluent boundary layers, and flow transition [1]. The authors research is pushing the boundaries of the application of computational fluid dynamics (CFD) technique in aircraft aerodynamic design and analysis [2–9].

To advance the state of the art in predicting high-lift flows, an open international workshop series (HiLiftPW) was established [10–12]. Geometries, numerical grids, and experimental results are publicly released before the workshop date. Participants are also invited to submit their own grids. The first two events highlighted the need to include high lift devices brackets and fairing in the models. In the third and last workshop, held in June 2017 in Denver, Colorado, two models were presented: the NASA High Lift Common Research Model (HL-CRM) and the Japanese JAXA Standard Model (JSM). Both are representative of realistic high-lift swept-wing aircraft (a typical 100-passenger class regional jet airliner) in landing configuration, but only for the latter experimental data were available.

Results of the third workshop were summarized in Ref. [12], which highlighted that: the wind tunnel model was mounted on a 60 mm stand-off without transitional strips, whereas simulations were required to be "free-air" and fully-turbulent, although optional transition modelling was permitted after the conclusion of the required cases; a grid convergence study on the JSM was not required (usually it is), but the implementation of a grid-adapted solution was an option after the conclusion of the required cases; solutions that well predicted the lift coefficient did not keep the same accuracy level for the drag and moment coefficients; accurate prediction of the aerodynamic (global) coefficients may be results of wrong pressure and skin friction distribu-

tions, whose integrals coincide with experimental data; RANS equations may admit multiple solutions for strong separated flow; standard turbulence models well agreed in the linear range of the lift curve; complex turbulence models yielded the closest results to the experimental maximum lift coefficient.

The authors focused on the JAXA model to assess their numerical prediction capability – i.e. meshing, numerical schemes, high-performance computing requirements. To cope with the objective, Reynolds-averaged Navier-Stokes (RANS) aerodynamic analyses have been performed on the super-computing grid infrastructure SCoPE (Sistema Cooperativo per Elaborazioni Scientifiche multidisciplinari, http://www.scope.unina.it) of the University of Naples "Federico II". The test case chosen is the JSM without engine nacelle and pylon. More in detail, the model geometry is a wing-body with high lift devices deployed, with a single segment baseline slat and a single segment 30° flap, including support brackets.

The aim of this work is to derive best practices for meshing and analysis with the lowest possible number of cells, giving indications on physics modelling and on the location of grid refinements for mesh tuning. Main results are shown in terms of aerodynamic coefficients, focusing on the prediction of the max value of the lift coefficient and its angle of attack, as well as on the flow behavior in stall condition. Post-process data also include pressure coefficient contours and streamlines to compare the numerical predicted vortices with the experimental data obtained in the 6.5 m by 5.5 m JAXA low-speed wind tunnel, obtained through the 3rd AIAA HiLiftPW website (https://hiliftpw.larc.nasa.gov/).

Section 2 describes the numerical models used throughout the simulations. A discussion on numerical results and their comparison with experimental data is given in Section 3. Conclusions are drawn in Section 4.

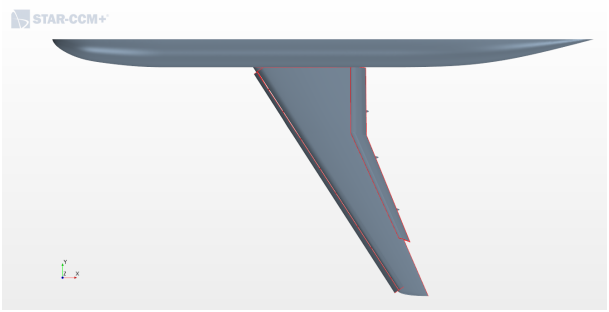

(a) *JAXA Standard Model geometry, top view.*

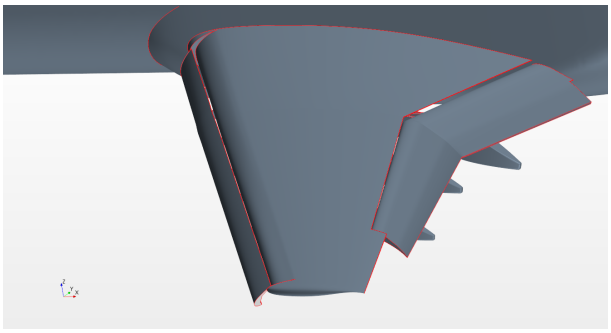

(b) *JAXA Standard Model geometry, wing detail.*

Fig. 1 JAXA Standard Model geometry.

2 Numerical model

The wing-body geometry is represented in Fig. 1. The numerical domain is externally bounded by a cuboid block, representing the farfield, and internally bounded by the aircraft surfaces. The aircraft is a half-model located on the block longitudinal symmetry plane. Taking as reference length the wing mean aerodynamic chord (mac), the block dimensions have been defined to get a distance from the aircraft equal to 90 mac for the inlet boundary and about 180 mac for the outlet boundary, about 45 mac for the lateral and the top/bottom boundaries.

The flow is modelled as an ideal, time-independent, compressible, and fully-turbulent gas. Data are shown in Table 1. All CFD simulations were "free-air" and the turbulence is modelled with the Spalart-Allmaras equation [13]. Furthermore, a set of simulations have been run with the Shear Stress Transport turbulence model by Menter [14] to assess the influence of the physics modelling on the aerodynamic coefficients for a high lift configuration. More details

Table 1 Flow conditions.

M_∞	p_∞ (Pa)	T_∞ (K)	Re (mac)
0.172	99680	306	1.93×10^6

are provided in the next section.

A large number of different polyhedral meshes have been investigated to achieve the best set-up. The main parameters are summarized in Table 2. Figure 2 shows some different details of the more refined mesh (ID 7 in Table 2).

The numerical simulations have been performed with STAR-CCM+ on the University's grid computing infrastructure SCoPE to simulate many configurations in a reasonable amount of time. The typical computational time with the number of central processing units (CPUs) is shown in Fig. 3, regarding simulations very similar to those discussed in this paper. It is apparent that to deal with refined meshes at least 32 CPUs are necessary. A typical computational time for the more refined grid discussed in this paper, with a mesh of more than 25 million cells, 128 CPUs, and 5000 iterations per angle of attack, is two days.

3 Numerical results

In this section, numerical results are summarized and discussed. In Fig. 4, the aerodynamic coefficients of the refined meshes (ID 5 to 7) are compared to the experimental data. As concern lift coefficient, a good agreement is clearly visible in the linear range of the curves and up to 10° angle of attack the relative error is below 3%. Therefore the lift curve slope is well estimated by all the numerical simulations. Instead, at higher angles of attack, numerical simulations cannot correctly predict the flow field, anticipating the separation and underestimating the maximum lift coefficient and the angle of stall. The degree of the numerical approximation depends on the mesh settings. The more refined mesh (ID 7) provides the best value of the max lift coefficient $C_{L_{\max}}$, because of local grid refinements on the wing leading edge, prism layer (boundary layer volume),

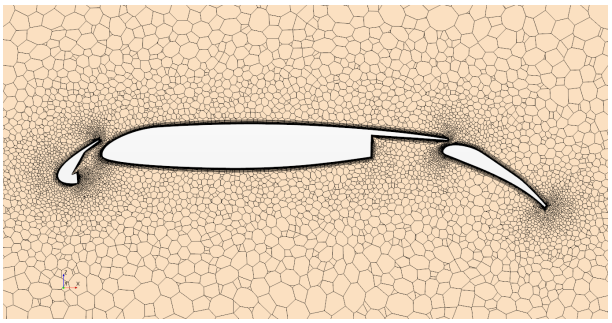

(a) *Wing section.*

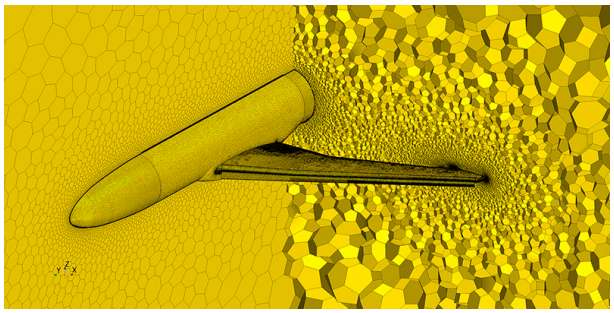

(b) *Distribution of polyhedral cells.*

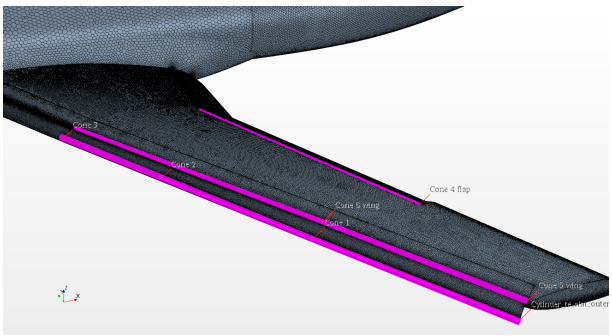

(c) *Volumetric controls.*

Fig. 2 Volume mesh on the model, grid ID 7.

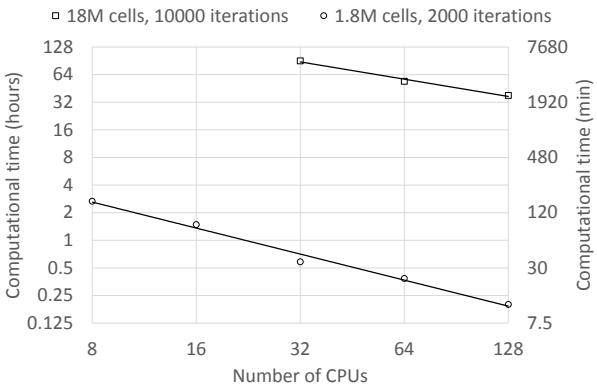

Fig. 3 Typical computational time.

Table 2 Mesh refinement resume.

ID	Cells no.	Notes
0	8.0×10^6	Initial mesh.
1	9.4×10^6	Refinement on wing, high lift devices, first (boundary) layer thickness.
2	11.2×10^6	Refinement on fuselage and high lift devices. Achieved dimensionless wall distance $y^+ \approx 1$.
3	14.9×10^6	Refinement on far-field and lifting surfaces. Decreased volume grow rate.
4	15.1×10^6	Customization of slat with respect to the expected slat cells width. Refinement on fuselage, on the prismatic (boundary) layer first and total thickness.
5	15.4×10^6	Refinement on trailing edges and slat support.
6	21.6×10^6	Refinement on slat, especially on the leading edge. All trailing edges have at least 4 cells in thickness.
7	26.4×10^6	Refinement on all leading edges, slat supports, and wing-tip. Increase in prism layer total thickness. Slight coarsening of the wing typical cells width. Final mesh.

and slat brackets (Fig. 5), but such value is underestimated by 0.25, with a 9% relative error, and the angle of stall is underestimated by 4°, with a 20% error. This is due to mispredicted separation phenomena occurring at the outer part of the wing, i.e. an inaccurate modelling of the vortices behind the outer slat brackets, as shown next.

The drag coefficient C_D is over-predicted in all simulations, yet the results are consistent, tending to the experimental data with increasing grid refinements. The relative error on the best mesh so far grows from 10% in the linear lift range to 25% at stall, which means an overestimate of about 200 drag counts at AOA $= 10°$ and $C_L = 2.2$.

The trend of the pitching moment coefficient C_M curve is slightly different, because of the effect of the flow separation that involves a different aerodynamic load and hence a different pitching moment distribution along the wing span. The relative error passes from 3% (a small overestimation in magnitude) at low angles of attack to -50% at AOA $\approx 16°$, due to the anticipated, numerical stall.

To understand where the numerical prediction fails, the available wind tunnel oil flow images have been compared with the wall shear stress distributions calculated with STAR-CCM+. Figures 6 and 7 show such comparison at 10.47° and 18.58° angles of attack, respectively. The similarity between the experimental pattern and the numerical prediction at AOA $= 10.47°$ in Fig. 6 is encouraging, since it means that the agreement on the integral aerodynamic coefficients is not a coincidence, but it is due to a good estimation of pressure and skin friction distributions. As expected from the aerodynamic coefficient curves, Fig. 7 shows that the numerical simulation at AOA $= 18.58°$ provides an anticipated separation starting from the outer slat brackets and extending spanwise downwind. The phenomenon initially happens on the last slat bracket, close to section H, at AOA $\approx 16°$, not shown here for brevity.

The same agreement is reported for the pressure coefficient C_p on the highlighted sections E, G, and H in Figs. 8 and 9. At the lower angle of attack, the numerical distribution is overlapped to the experimental data. At AOA $= 18.58°$, the simulation predict a completely separated flow on these wing sections.

To highlight the effects of the slat brackets on the wing stall, a set of simulations have been performed on the JSM configuration without brackets. In Fig. 10, the skin friction coefficient is depicted to display the separated flow zone behind

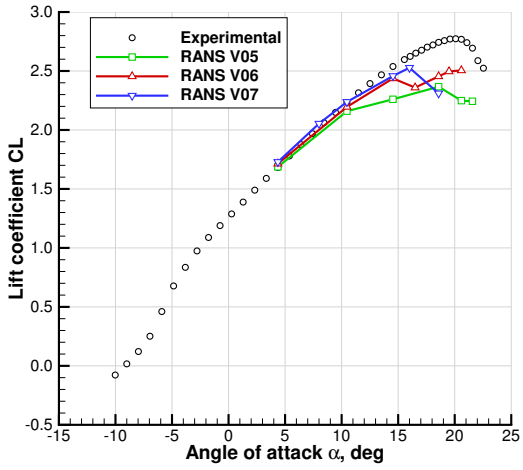

(a) Lift curve.

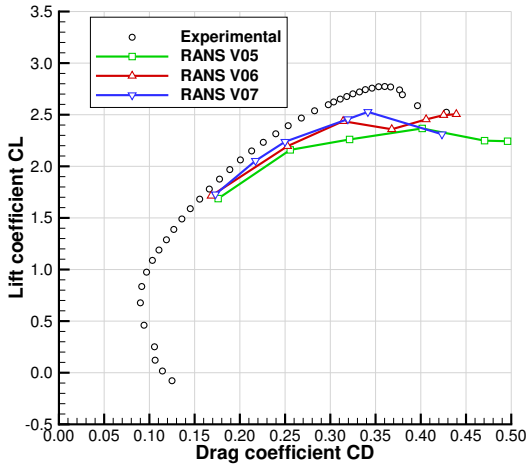

(b) Drag polar.

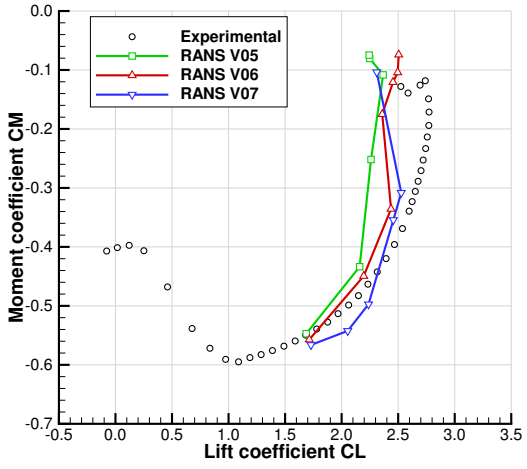

(c) Pitching moment curve.

Fig. 4 Numerical vs experimental results, SA turbulence model.

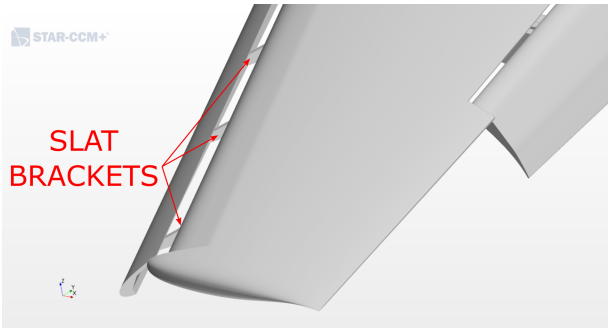

Fig. 5 Slat brackets.

the brackets. The aerodynamic coefficients are reported in Fig. 11. The lift coefficient is well estimated (numerical and experimental data are overlapped) except at the stall, which occurs at a higher angle of attack and a higher $C_{L_{\max}}$ value. Even in this case, the drag coefficient is slightly over-predicted. The moment coefficient is over-predicted in magnitude for any value of the lift coefficient. As highlighted at the first AIAA HiLiftPW [10], the effects of the slat tracks cannot be neglected.

An inviscid, Eulerian analysis has also been performed to estimate the $C_{L_{\max}}$ achievable with a simple simulation and a reduced number of cells (2.2 million, without prism layer, since there is no boundary layer). From the lift curve of Fig. 12a, it may be assumed, as a rule of thumb, that the viscous stall occurs:

$$\text{at } \mathrm{AOA}_{\text{stall}} = \mathrm{AOA}_{\text{stall EULERIAN}} - 5^\circ;$$

$$\text{with } \mathrm{C}_{L_{\max}} = C_{L_{\max\,\text{EULERIAN}}} - 0.50.$$

As expected, the lift curve slope is the only curve characteristic well predicted. The lift coefficient at zero angle of attack C_{L_0} is overestimated by 0.2. Probably, the angle of zero lift is overestimated in magnitude by 2°-3°. The stall at AOA = 24° is due to pressure separation phenomena. The drag polar is close to the experimental data because of the higher lift and lower drag predicted by this model – a mere coincidence. The pitching moment coefficient is strongly over-predicted in magnitude.

Finally, a set of simulations have been performed with the Menter's Shear Stress Transport

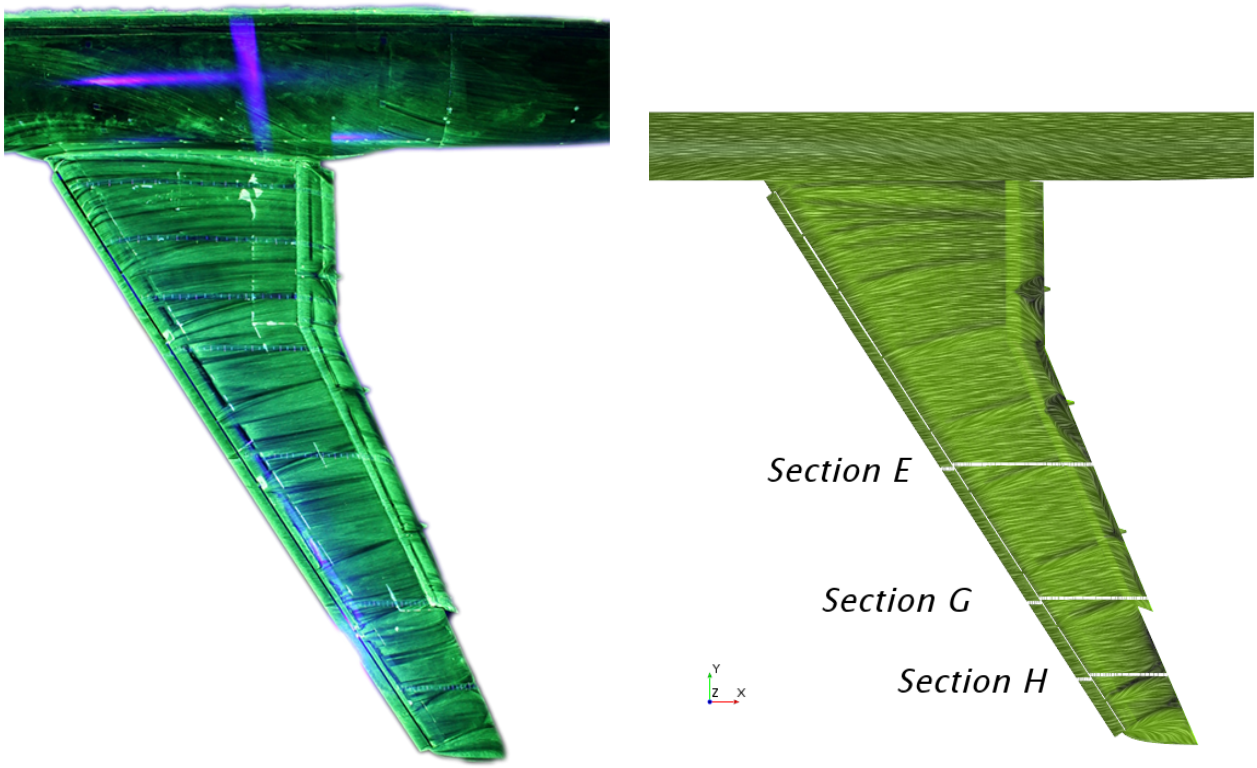

(a) Oil flow (wind tunnel). (b) Wall shear stress (CFD V07).

Fig. 6 Shear stress distribution at AOA = 10.47°.

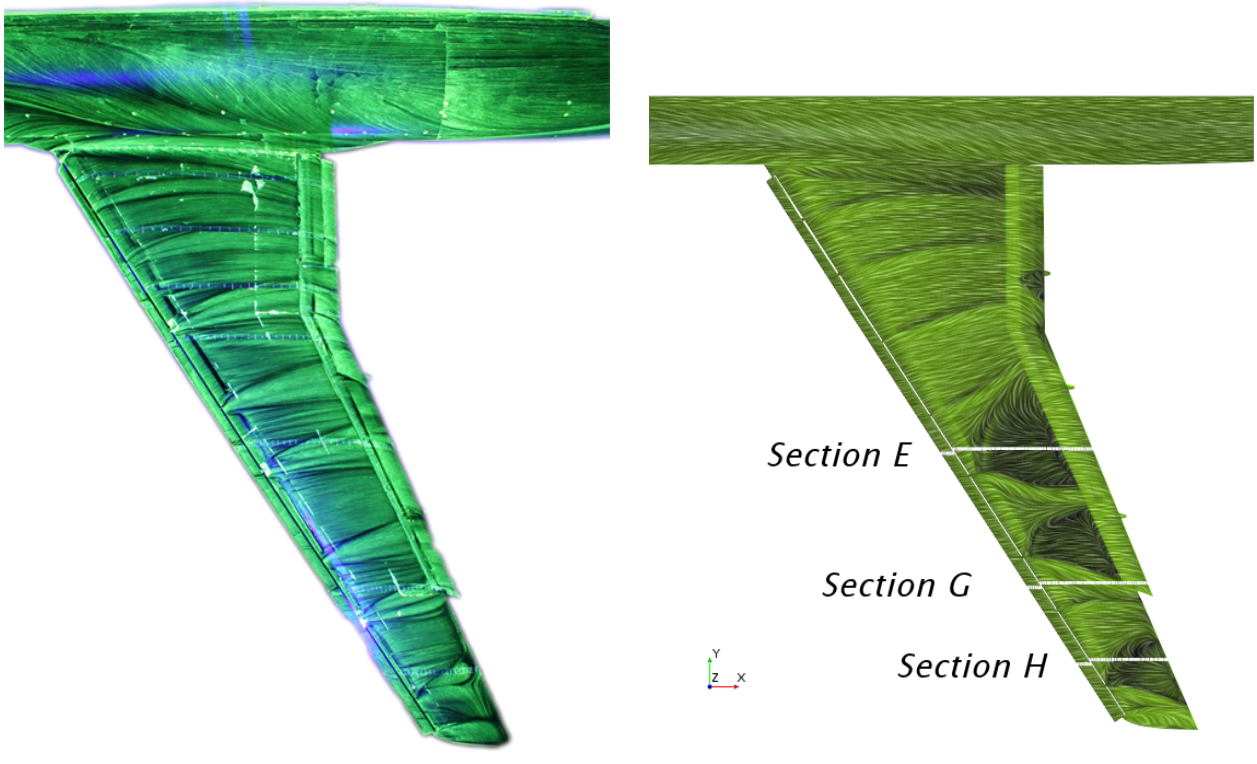

(a) Oil flow (wind tunnel). (b) Wall shear stress (CFD V07).

Fig. 7 Shear stress distribution at AOA = 18.58°.

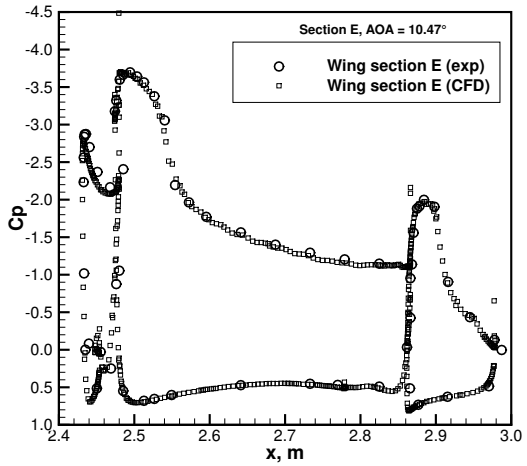

(a) Section E.

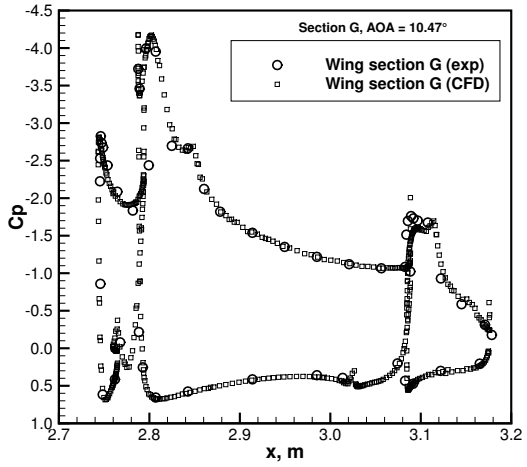

(b) Section G.

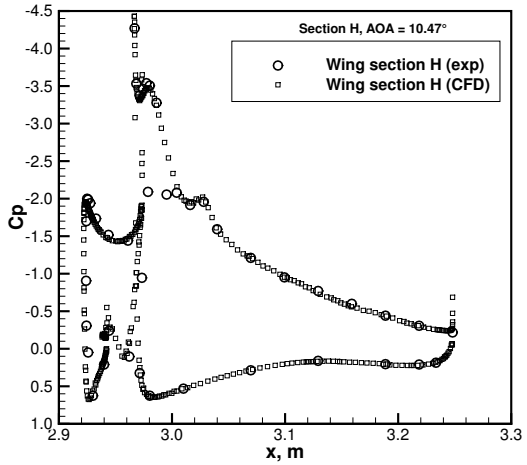

(c) Section H.

Fig. 8 Numerical vs experimental pressure coefficient at several span sections, AOA = 10.47°.

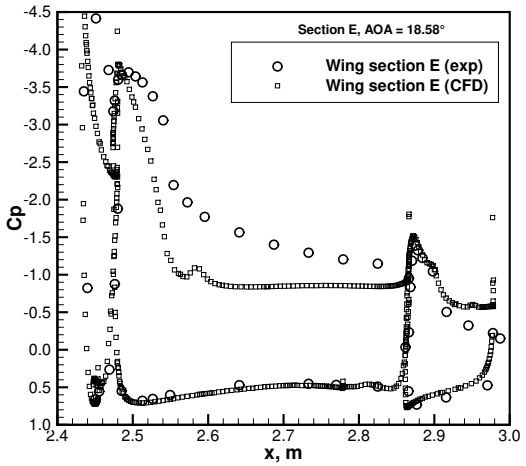

(a) Section E.

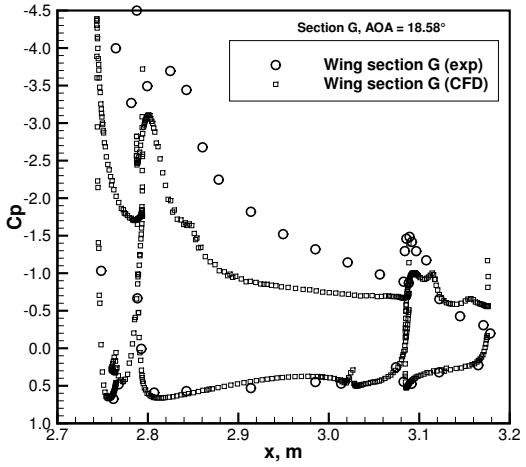

(b) Section G.

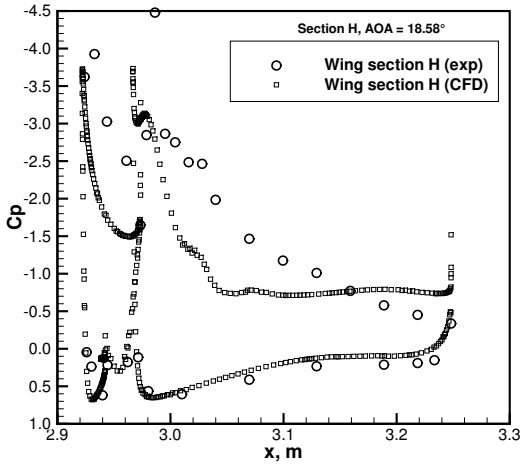

(c) Section H.

Fig. 9 Numerical vs experimental pressure coefficient at several span sections, AOA = 18.58°.

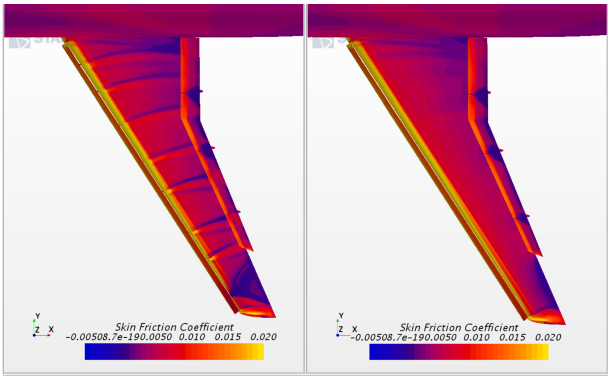

Fig. 10 Configuration with (left) and without (right) slat brackets, comparison of skin friction coefficient, AOA = 16°.

turbulence model [14], known also as K-ω SST, to assess the influence of the physics modelling on the aerodynamic coefficients. The flow is simulated fully-turbulent. From the coefficients reported in Fig. 13, it is possible to conclude that the results do not change with the SST turbulence model, except for a small reduction in magnitude of the C_M before the stall, within 3% from the SA model.

4 Conclusion

The main aim of this work was to provide best practices for numerical meshing and analysis with the lowest possible number of cells, giving indications on physics modelling and on the location of grid refinements for mesh tuning. To cope with the objective, several grids were generated by the authors. Numerical results have been compared in terms of global aerodynamic coefficients, section pressure coefficient, and shear stress distribution. Particular attention was payed on computational time. Although it depends on several parameters, such as hardware characteristics, number of CPUs available, and numerical parallelization scheme, a crucial item is the number of cells. In our analyses, the finest mesh is made of 26.4×10^6 cells, whereas participants at the 3rd AIAA HiLiftPW [12] have used more than twice the number of cells. Therefore, it is reasonable to conclude that the mesh settings applied by the authors may provide a significant reduction

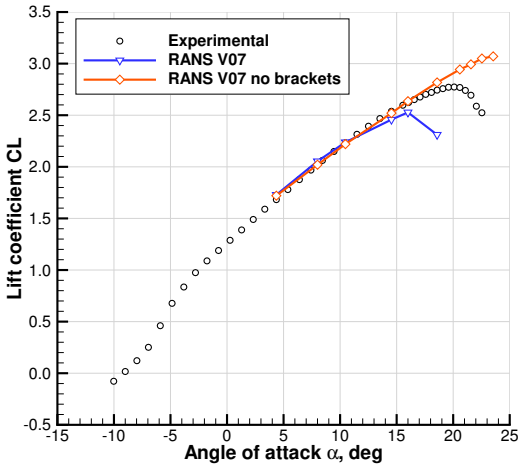

(a) Lift curve.

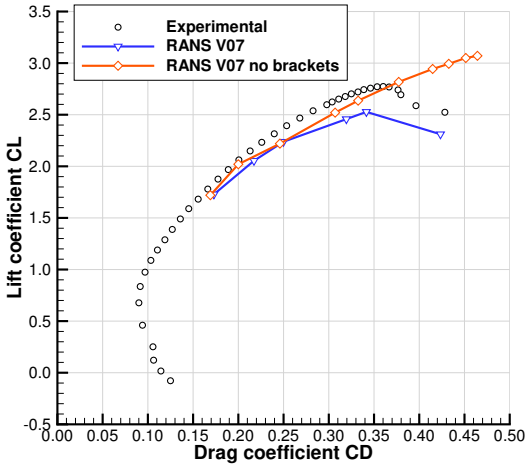

(b) Drag polar.

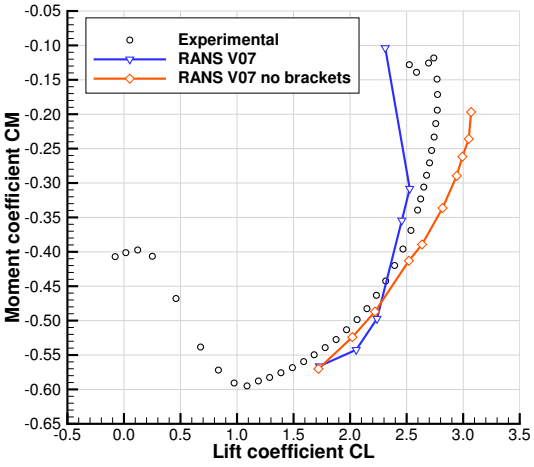

(c) Pitching moment curve.

Fig. 11 Effects of the slat brackets.

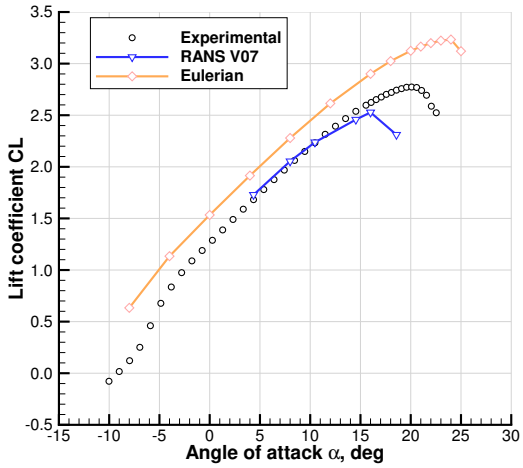

(a) Lift curve.

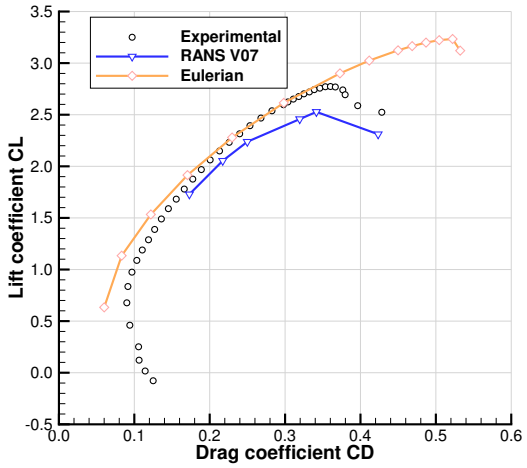

(b) Drag polar.

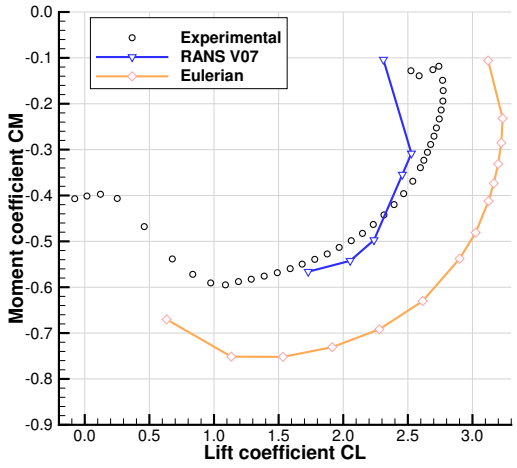

(c) Pitching moment curve.

Fig. 12 Comparison among experimental, RANS (SA turbulence model), and Eulerian results.

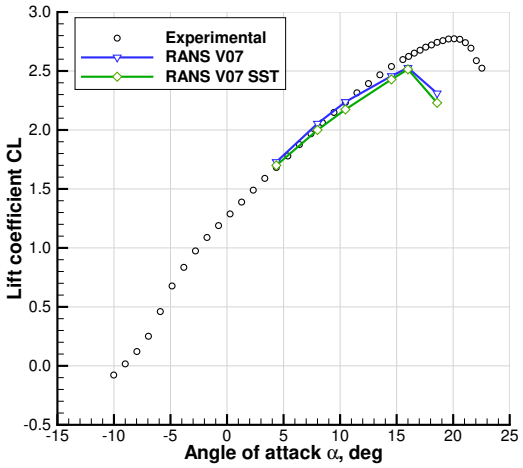

(a) Lift curve.

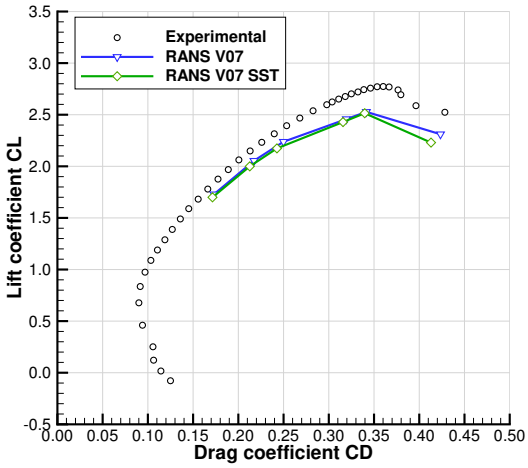

(b) Drag polar.

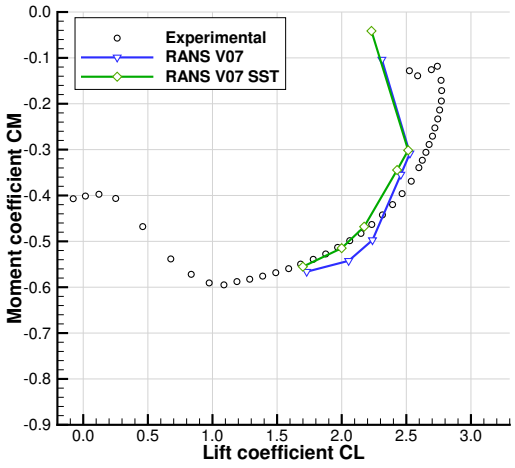

(c) Pitching moment curve.

Fig. 13 Effect of the turbulence model: one-equation SA model vs two-equations SST model.

in computational time. The actual CPU time to achieve convergence on the finest mesh is about 50 hours for each angle of attack.

From this work and the authors experience it follows that the mesh should be a very good representation of the geometry, especially on curved surfaces exposed to the upwind stream, as the leading edges of the lifting surfaces. The aspect ratio of the prism layer cells should be close to unity, the total layer height bigger than the expected boundary layer thickness, a number from 20 to 50 layers. Trailing edges should have at least 2 cells along their thickness, ideally 8. Slat and flaps tracks should be treated with the same or better accuracy of the high lift devices. A surface refinement propagating in the volume with a grow rate of 1.05 (next cell is 5% bigger than the previous one) is often sufficient to catch the main phenomena. The volume mesh in the slots may be refined as long as the leading edges are well represented. Wake refinements may be not always necessary, especially if there are no surfaces downstream. The farfield block should be big enough to be far from the body, say 100 chords length ahead and 200 chords length behind. Its boundaries should not be too coarse, say a cell size of about 4 chord length, allowing a few hundreds cells on the boundary surfaces.

As stated in the previous section, the difference between numerical and experimental values of $C_{L_{\max}}$ is related to inadequate resolution of flow structures originating from the outer brackets, as well as of the wake of the relative sections. Further investigation are currently under consideration with a finer mesh, which includes refinements on the wake of the slat tracks.

Finally, it has been demonstrated that the numerical results are independent from the turbulence model, at least for the grids considered.

References

[1] Della Vecchia P, Ciliberti D. Numerical aerodynamic analysis on a trapezoidal wing with high lift devices: a comparison with experimental data. *22nd AIDAA Conference*, Naples, Italy, 2013.

[2] Ciliberti D, Della Vecchia P, Nicolosi F, and De Marco A. Aircraft directional stability and vertical tail design: A review of semi-empirical methods. *Progress in Aerospace Sciences*, Vol. 95, pp 140-172, 2017. https://doi.org/10.1016/j.paerosci.2017.11.001

[3] Nicolosi F, Ciliberti D, and Della Vecchia P. Aerodynamic Design Guidelines of Aircraft Dorsal Fin. *34th AIAA Applied Aerodynamics Conference*, Washington, D.C., AIAA 2016-4330, 2016. https://doi.org/10.2514/6.2016-4330

[4] Della Vecchia P, Stingo L, and De Marco A. An improved method for transport aircraft for high lift aerodynamic prediction. *Aerospace European 6th CEAS Conference*, No. 254, Bucharest, Romania, 2017.

[5] Nicolosi F, Della Vecchia P, Ciliberti D, and Cusati V. Fuselage aerodynamic prediction methods. *Aerospace Science and Technology*, Vol. 55, pp 332-343, 2016. https://doi.org/10.1016/j.ast.2016.06.012

[6] Della Vecchia P, and Nicolosi F. Aerodynamic guidelines in the design and optimization of new regional turboprop aircraft. *Aerospace Science and Technology*, Vol. 38, pp 88-104, 2014. http://dx.doi.org/10.1016/j.ast.2014.07.018

[7] Nicolosi F, Della Vecchia P, Ciliberti D, and Cusati V. Development of new preliminary design methodologies for regional turboprop aircraft by CFD analyses. *29th Congress of the International Council of the Aeronautical Sciences*, Saint Petersburg, Russia ICAS 2014-0407, 2014.

[8] Nicolosi F, Della Vecchia P, and Corcione S. Aerodynamic analysis and design of a twin engine commuter aircraft. *28th Congress of the International Council of the Aeronautical Sciences*, Brisbane, Australia, pp 321-332, 2012.

[9] Pascale L, and Nicolosi F. Design and aerodynamic analysis of a light twin-engine propeller aircraft. *26th Congress of International Council of the Aeronautical Sciences*, Anchorage, Alaska, pp 3890-3904, 2012.

[10] Rumsey CL, Slotnick JP, Long M, Stuever RA and Wayman TR. Summary of the First AIAA CFD High-Lift Prediction Workshop.

Journal of Aircraft, Vol. 48, No. 6, pp 2068-2079, 2011. https://doi.org/10.2514/1.C031447

[11] Rumsey CL and Slotnick JP. Overview and Summary of the Second AIAA High-Lift Prediction Workshop. *Journal of Aircraft*, Vol. 52, No. 4, pp 1006-1025, 2015. https://doi.org/10.2514/1.C032864

[12] Rumsey CL, Slotnick JP, and Sclafani J. Overview and Summary of the Third AIAA High Lift Prediction Workshop. *2018 AIAA Aerospace Sciences Meeting, AIAA SciTech Forum*, Kissimmee, Florida, AIAA 2018-1258, 2018. https://doi.org/10.2514/6.2018-1258

[13] Spalart PR and Allmaras SR. A one equation turbulence model for aerodynamic flows. *AIAA Journal*, Vol. 94, 1992.

[14] Menter FR. Two-Equation Eddy-Viscosity Turbulence Models for Engineering Applications, *AIAA Journal*, Vol. 32, No. 8, pp 1598-1605, 1994.

Contact Author Email Address

The corresponding author, V. Cusati, can be contacted at the following address:
vincenzo.cusati@unina.it

Copyright Statement